# Coda wave interferometry in monitoring the fracture process of concrete beams under bending test

**Magdalena KNAK** ⓘ*, **Erwin WOJTCZAK** ⓘ, and **Magdalena RUCKA** ⓘ

Department of Mechanics of Materials and Structures, Faculty of Civil and Environmental Engineering, Gdańsk University of Technology,
Narutowicza 11/12, 80-233, Gdańsk, Poland

**Abstract.** Early detection of damage is necessary for the safe and reliable use of civil engineering structures made of concrete. Recently, the identification of micro-cracks in concrete has become an area of growing interest, especially when it comes to using wave-based techniques. In this paper, a non-destructive testing approach for the characterization of the fracture process was presented. Experimental tests were performed on concrete beams subjected to mechanical degradation in a 3-point bending test. Ultrasonic waves were registered on a specimen surface by piezoelectric transducers located at several points. Then, the signals were processed taking advantage of wave scattering due to micro-crack disturbances. For early-stage damage detection, coda wave interferometry was used. The novelty of the work concerns the application of the complex decorrelation matrix and the moving reference trace approach for better distinguishment of sensors located in different parts of a crack zone. To enhance coda wave-based damage identification results, optical imaging of crack development was performed by means of digital image correlation measurement. The results obtained showed that the coda wave interferometry technique can be successfully used as a quantitative measure of changes in the structure of concrete. The results also indicated that the course of decorrelation coefficient curves enabled the identification of three stages during degradation, and it depended on the location of acquisition points versus the crack zone.

**Key words:** non-destructive testing; concrete beams; crack detection; fracture process; ultrasonic waves; coda wave interferometry; digital image correlation.

## 1. INTRODUCTION

Concrete elements such as beams are widely used in engineering structures. For the safety of use, it is important to verify the material condition, detect existing damage and prevent its future growth. An essential aspect that needs to be mentioned here is the observation of micro-cracks, which indicate incipient damage. Micro-cracks are external or internal micro-damage caused by the growth of stress in the structure. They appear before visible fracture of the element, at the stress level lower than the strength of the material. The occurrence of micro-cracks signals the emergence and potential development of larger macro-damage, which may lead to more serious consequences. Thus they can be used as an early-stage indicator of fractures.

Nowadays, non-destructive testing (NDT) techniques provide the possibility to observe the current state of an element without impairing its internal structure. There are many NDT methods used by researchers. Among others, the techniques taking advantage of elastic wave propagation are very successful in monitoring the condition of engineering structures, which was proved by numerous works (e.g. [1–7]). A promising approach based on ultrasonic waves is coda wave interferometry (CWI). The method utilizes the fact that ultrasonic waves

propagating in heterogenous media (such as concrete) are very sensitive to changes in the structure of the medium. In the intact material, the waves propagate through the element and partially scatter at the inhomogeneities of the medium, resulting in so-called diffusive waves (coda waves). In the case of any disturbance (e.g. micro-cracks) that slightly alters the configuration of the components (e.g. grain, cement, pores), the wave scattering is different and the coda waves change, even though the recorded ultrasonic signals appear to be generally similar. The differences may include, for example, translation or stretching of the waveforms. The quantitative measure of this change is provided by the decorrelation between the reference and disturbed signal. This approach was successfully used in several works (e.g. [8–15]). The effectiveness of the diffuse ultrasound method for micro-cracking detection in concrete was studied by Ahn *et al.* [11]. Their work focused on finding the appropriate frequency range to characterize micro-cracking in concrete specimens. Sang *et al.* [12] used CWI to quantify fatigue damage and failure precursors in cylindrical specimens of shale. Detecting local damage with nonlinear CWI was also considered by Smagin *et al.* [13]. The researchers used the nonlinear modification of CWI and time-reversal techniques to focus on a selected area, where the damage occurred.

A recent trend in non-destructive testing is the support of wave-based methods with optical imaging of cracks development during mechanical degradation. One of the methods used for this purpose is digital image correlation (DIC), which al-

*e-mail: magdalena.knak@pg.edu.pl

lows for localizing structural damage (e.g. cracks) by observing the local changes in strains and displacements. In previous studies, the DIC method was successfully used to monitor the growth of the damage, e.g. crack height or width [16–24]. Some of the researchers used integrated ultrasonic and DIC techniques, confirming the high efficiency of such an approach. Wojtczak *et al*. [14] further proved it in their research with additional analysis of X-ray micro-computed tomography during a splitting test. The use of integrated methods allowed for monitoring of the fracture process and early damage detection of concrete cubes. DIC measurements in combination with acoustic emission (AE) and dynamic identification were examined by Lacidogna *et al*. [22]. This multi-technique damage monitoring was conducted on four dimensional scales of concrete beams to emphasize the scale effect and its influence on damage detection.

This paper presents a scheme of non-destructive testing of concrete beams under the three-point bending test. The fracture process was described using the characteristics of ultrasonic waves registered at several points on a specimen surface by piezoelectric transducers. For early-stage damage detection, coda wave interferometry was used. The novelty of the work concerns the application of the complex decorrelation matrix and the moving reference trace approach for better distinguishment of sensors located in different parts of a crack zone. The results of micro-cracks detection obtained by means of the coda wave interferometry approach were successfully verified by the digital image correlation technique.

## 2. MATERIALS AND METHODS

### 2.1. Object of research

Experimental analysis was carried out on three concrete beams (#1–#3), each with the dimensions of $40 \times 40 \times 160$ mm$^3$. The specimens were notched in the central part to induce crack formation in the region of interest. The notch had a width of 4 mm and depth of 7 mm and was made in the middle of the beam (Fig. 1a).
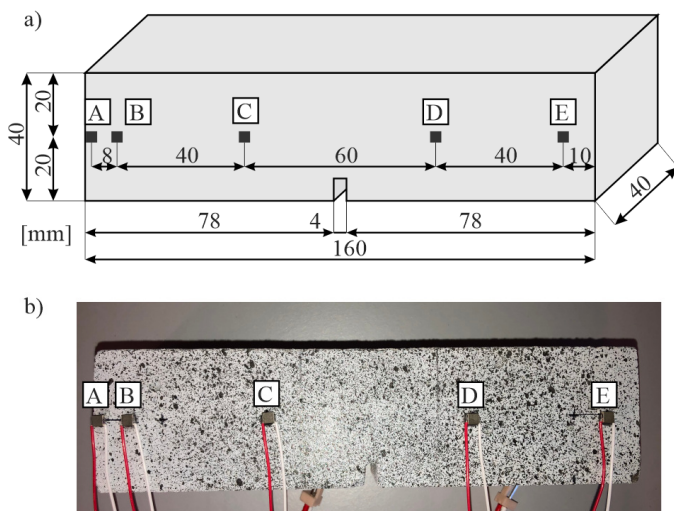


**Fig. 1.** Tested specimens: a) geometry and location of transducers, b) photograph of example specimen with speckle pattern

All beams were made of a concrete mix prepared from the following composition: CEM I 42.5R (450 kg/m$^3$), water (177 kg/m$^3$), sand 0–2 (675 kg/m$^3$) and gravel 2–8 (675 kg/m$^3$). The surface of specimens was covered with a speckle pattern (Fig. 1b) to make DIC measurements possible. Firstly, a layer of white paint was applied. After that, a random pattern was added by spraying the surface with black paint.

### 2.2. Experimental procedure

The experimental setup incorporated in the current study is shown in Fig. 2. The three-point bending test was carried out on concrete beams #1–#3 with the use of the Zwick/Roell Z10 universal testing machine. Support spacing was assumed to be equal to 12 cm. The preload applied to the specimen was 20 N. Loading was performed with a constant displacement increase equal to 0.05 mm/min. The test stopped after 600 s when the 0.5 mm displacement was reached.
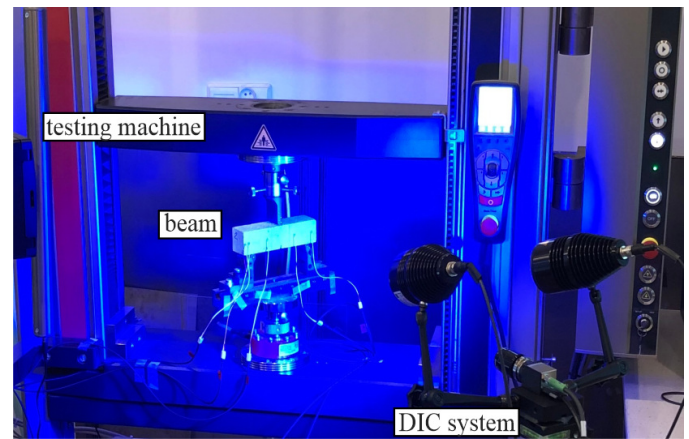


**Fig. 2.** Experimental setup

During the test, the ultrasonic signals were registered by five Noliac piezoelectric transducers with the dimensions of $3 \times 3 \times 3$ mm$^3$ (Fig. 1b). One of them acted as an actuator (A) and the rest of them were sensors (B–D). The excitation was a wave packet composed of a 5-cycle sine wave modulated by the Hann window. The central frequency of the wave packet was set as 500 kHz. Excitation of the signal was provided by an arbitrary AFG3022C waveform generator supported by an AB A400DI high voltage amplifier. The ultrasonic waves were excited and registered with an interval of 1 s. The signals were collected during measurements for further processing by the CWI method.

Simultaneously with the ultrasonic measurements, digital image correlation was applied. In the study, the photographs of the specimens were taken using the ARAMIS MC 2D 12M system, with a fixed time step equal to 1 s. The collected pictures were then processed using the Aramis Professional software. Each subsequent image was compared to the reference one, taken in the intact state. In such a manner, changes in the motion of pixel groups were recorded and the displacements/deformations were calculated, allowing one to observe the change of strain and crack evolution.

2

*Bull. Pol. Acad. Sci. Tech. Sci.*, vol. 71, no. 3, p. e144118, 2023

## 2.3. Coda wave interferometry

The CWI method is extremely effective in detecting damage in heterogeneous materials, such as micro-cracks in concrete. If there are even slight changes in the structure of the tested object, the propagation of the wave is influenced and the information about these events is located in the 'tail' of the signal, i.e. in the coda wave range. Since coda is not equally present in the whole signal range, the first step is to define its time duration. To specify this, each signal is divided into small intervals. Then, from each of these parts, DC is calculated according to equation (1). This makes it possible to determine in which interval the coda wave occurs. As the next step, the decorrelation between specific pairs of waveforms in a specified time range is calculated. The particular reference signal $s_i(t)$ is compared to another signal $s_j(t)$. Indices $i$ and $j$ refer to the signal numbers. Differences between the signals are expressed by the so-called decorrelation coefficient (DC), calculated according to the following equation:

$$DC_{i,j} = 1 - \frac{\int\limits_{t_1}^{t_2} s_i(t) \cdot s_j(t)\, dt}{\sqrt{\int\limits_{t_1}^{t_2} s_i^2(t)\, dt \int\limits_{t_1}^{t_2} s_j^2(t)\, dt}},$$

$$i = 1, \ldots, n, \quad j = i, \ldots, n.$$

(1)

Multiple calculations of $DC$ for all potential waveform pairs in a dataset with $n$ signals allow for the formation of an $n \times n$ **DC** matrix given by:

$$\mathbf{DC} = \begin{bmatrix} 0 & DC_{1,2} & \cdots & DC_{1,n-1} & DC_{1,n} \\ 0 & 0 & \cdots & DC_{2,n-1} & DC_{2,n} \\ \vdots & \vdots & \ddots & \vdots & \vdots \\ 0 & 0 & \cdots & 0 & DC_{n-1,n} \\ 0 & 0 & \cdots & 0 & 0 \end{bmatrix}.$$

(2)

The classic approach uses the first row of the **DC** matrix, which allows to show only the decorrelation between the first signal (as reference) and all following signals (as the disturbed ones), without considering decorrelation changes between each consecutive pair of waveforms. However, bearing in mind that wave propagation signals are based on sine functions which are periodic, there exists a risk of underestimating the decorrelation if the translational difference between two signals is greater than the period, especially in the case of significant changes in the media (e.g. cracking). Thus, it is important to analyze the whole **DC** matrix in order to eliminate the above-mentioned cycle-skipping effect. A simple but robust solution to this problem is the so-called moving reference trace method (MRT) [25]. In this approach, the decorrelation includes changes between a particular signal and a set of preceding signals (not only the first one). Firstly, it is necessary to adopt a certain calculation step $k$, allowing to determine the number of reference signal $r$ for each particular $j$-th signal in the data set. For all signals numbered $j \leq k$, the first signal is taken as the reference, i.e. the values from the first row of the **DC** matrix are taken to the newly calculated **DC**$^{mrt}$ vector (without additional calculations). For each subsequent signal numbered $j > k$, a new reference signal number is calculated according to the formula:

$$r = k \cdot \left\lfloor \frac{j - 0.5}{k} \right\rfloor.$$

(3)

Then, the new element of the **DC**$^{mrt}$ vector is calculated as the sum of the previously calculated $r$-th value of **DC**$^{mrt}$ and the decorrelation between the currently analyzed $j$-th signal and the new reference $r$-th signal. The described procedure can be written with the formula below:

$$DC_j^{mrt} = \begin{cases} DC_{1,j} & j \leq k, \\ DC_r^{mrt} + DC_{r,j} & j > k, \end{cases}$$

(4)

$$\mathbf{DC}^{mrt} = \left\{ 0 \quad DC_2^{mrt} \quad \cdots \quad DC_n^{mrt} \right\}.$$

(5)

The calculation can be performed for successive values of $k = 1, \ldots, n$. Subsequently, a series of **DC**$^{mrt}$ vectors is obtained, which can be compiled into a single $n \times n$ **DC**$^{mrt,g}$ global matrix.

## 3. RESULTS AND DISCUSSION

### 3.1. Bending test

The results of the 3-point bending test are presented in Fig. 3. The peak load values for beams #1, #2 and #3 were: 2007 N, 2023 N and 2025 N, respectively. The mean value equaled 2018 N and standard deviation was 9.9 N, which resulted in a low coefficient of variation equal to 0.5%. Maximum forces were obtained for the following time instances: 335 s, 298 s and 376 s for beams #1, #2 and #3, respectively.
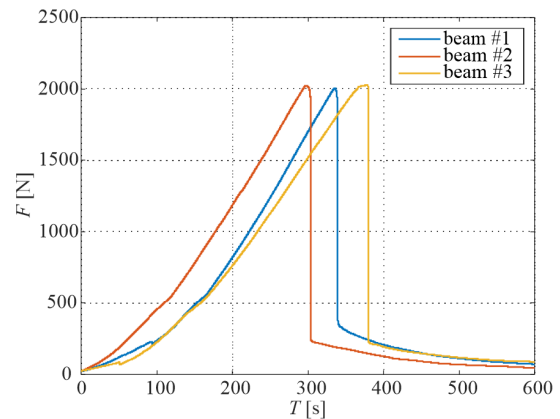


**Fig. 3.** Three-point bending test results: force-time diagram for beams #1–#3

### 3.2. Digital image correlation

The crack propagation was visualized by the photographs taken during the experimental procedure. The DIC technique allowed to monitor the surface component. Major strain maps for each beam were calculated. The images at different load levels for

all beams are illustrated in Fig. 4. The following steps were analyzed: the moment of initiation of the crack, the step at the load value equal to 90% of the maximum force before reaching the peak value (90% pre-peak), the step at the peak value, the step at the load value equal to 90% of the maximum force after reaching the peak value (90% post-peak), the step at the load value equal to 10% of the maximum force after reaching the peak value (10% post-peak) and the step at the end of the test.

The first occurrence of the fracture process zone (FPZ) is visible in Fig. 4a. In Table 1 appropriate times and percentages

of the peak values are given. For all beams, the first appearance of FPZ was at about 85% of the pre-peak value. The behavior of crack development for all beams was similar. The direction and curvature of the macro-crack depended on the heterogeneous structure of the material and on the occurrence of grains on the surfaces of specimens.

**Table 1**
Initiation of the fracture process zone

| Beam | $T$ [s] | $\%F_{max}$ |
|------|---------|-------------|
| #1   | 300     | 84          |
| #2   | 258     | 83          |
| #3   | 330     | 86          |

### 3.3. Coda wave interferometry

The experimental data obtained were processed using the procedure described in Section 2.3, with the use of the coda wave approach. At the beginning, each signal was divided into small parts with a duration of 0.01 ms. Then, for each of these parts, DC was calculated according to equation (1), treating the first signal as a reference one. This allowed for observing which part of the signal changed significantly over time, and thus contained the coda wave. Figure 5 presents the results of calcula-
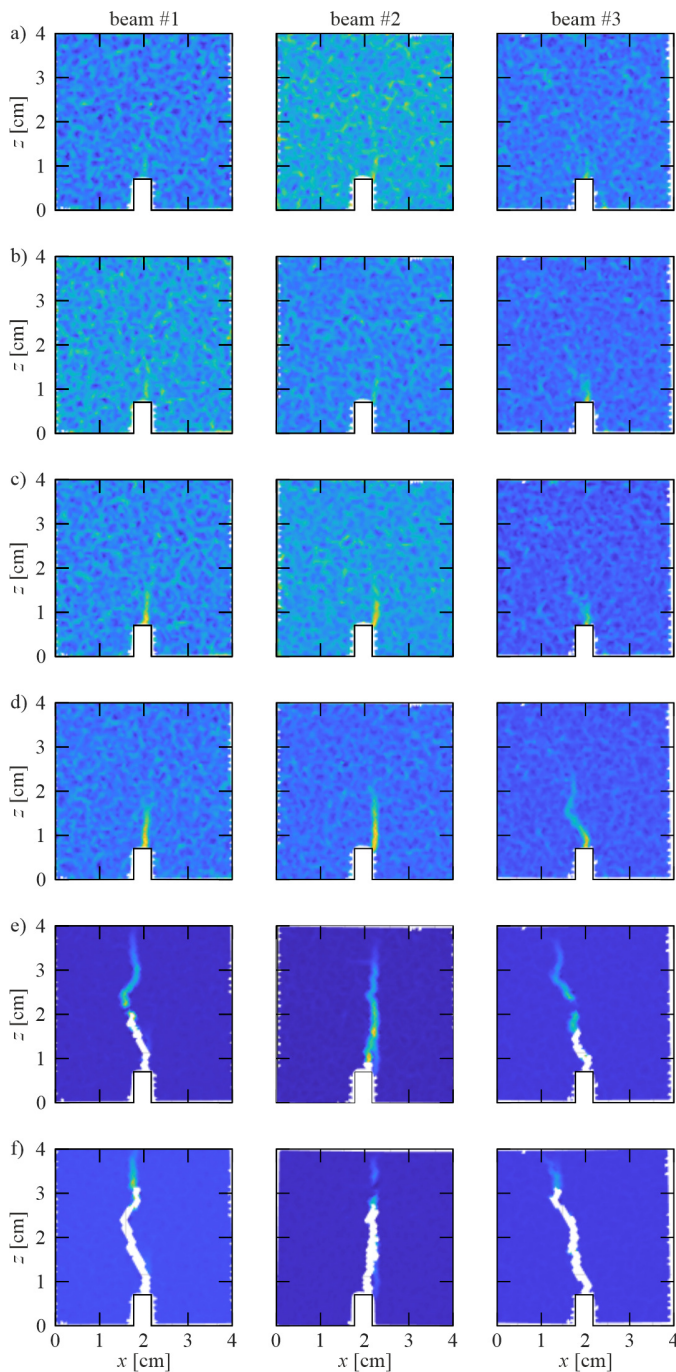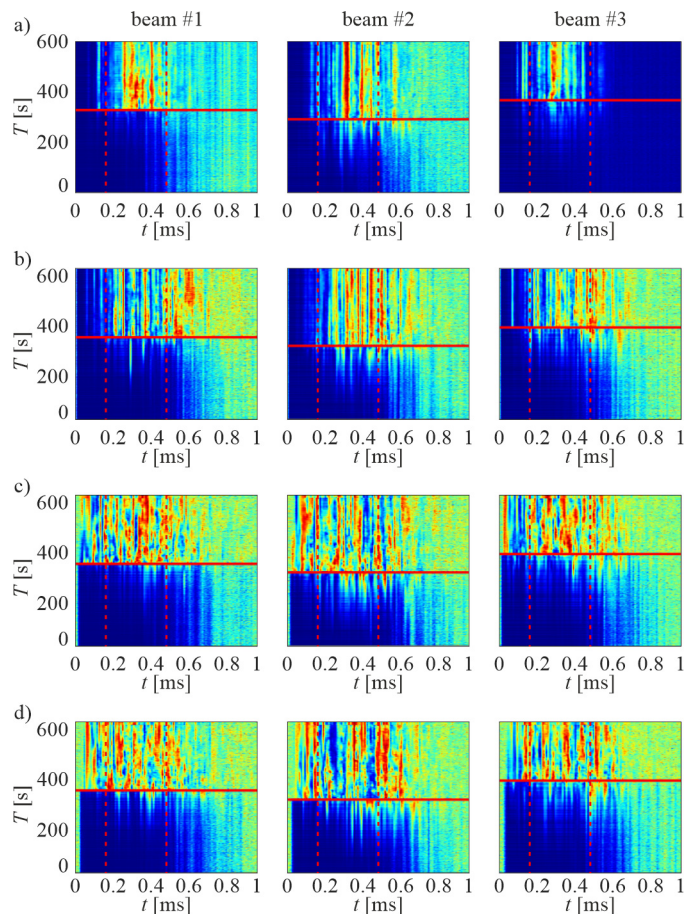


**Fig. 4.** DIC results of major strain for beams #1–#3 at different load levels in relation to force: a) initiation of crack, b) 90% pre-peak, c) peak value, d) 90% post-peak, e) 10% post-peak, f) end of the test



**Fig. 5.** Detection of time range of coda waves for beams #1–#3 and different sensors: a) sensor B, b) sensor C, c) sensor D, d) sensor E

tions for all beams (#1–#3) and sensors (#B–#E). In the diagrams, the vertical axis $T$ specifies the duration of the experiment and the horizontal axis $t$ is the time of a particular signal. It is evident that the highest DC values are observed in the time range of 0.2–0.5 ms (marked in the figure by vertical dashed lines), thus it will be used for further calculations.

After the determination of the coda wave range, full **DC** matrices were calculated. Then the moving reference procedure was applied with different steps $k$ to obtain global $\mathbf{DC}^{mrt,g}$ matrices. Figure 6 shows the changes in the decorrelation coefficient during the bending test. The DC values were calculated conventionally, taking the first signal as a reference for each consecutive signal. In the graph, the moment of maximum force occurrence is marked with a vertical red line. Three stages can be clearly determined, marked successively as S1, S2 and S3 in Fig. 6. The first stage (S1) is characterized by a slow increase in the DC coefficient, which corresponds to the initial stage of sample loading. It can be observed that in the initial loading stage, the decorrelation values are relatively low. Importantly, with the increasing loading, an increase in the DC value is evident, even though no visible damage appears on the object. This behavior indicates the formation of micro-cracks in the beams. In the S2 stage, the DC values increase rapidly. This effect is associated with obtaining the maximum force. After reaching the destructive force, a clear increase in the value of decorre-
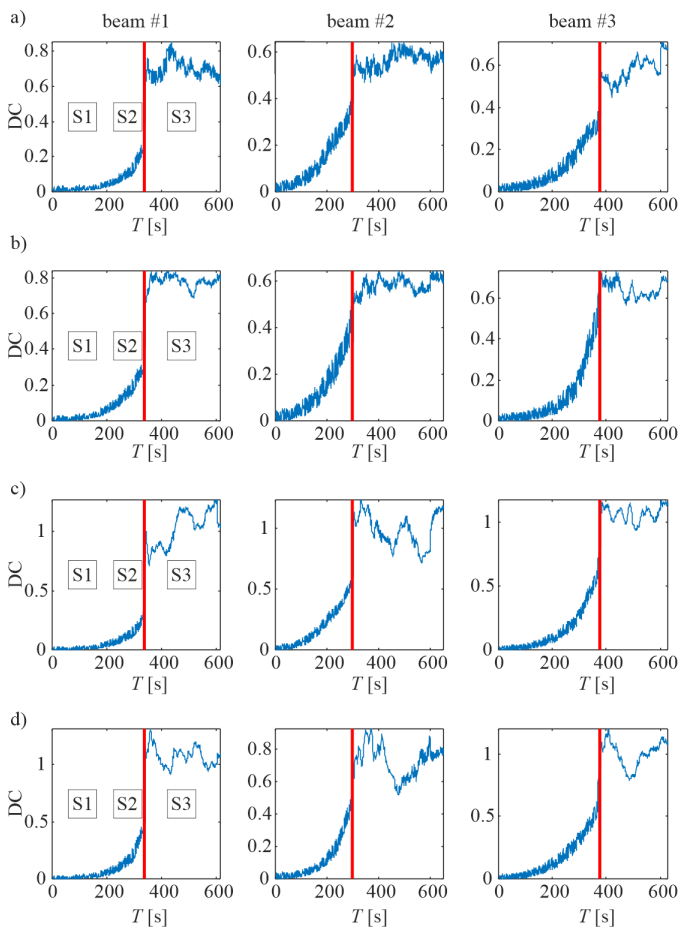
lation is observed, followed by stabilization at a higher level. Stage S3 corresponds to the moment of stabilization, associated with the occurrence of macro damage, i.e. an open crack. The changes in DC values appearing at this stage testify to the development of the occurring failure of the beams under consideration. When analyzing the graphs corresponding to each sensor, several issues can be noted. The results obtained for the sensors located in front of the crack (between the actuator and the crack, i.e. #B, #C) are burdened with visible noise. The noise makes it difficult to distinguish between different stages of damage. It is not possible to determine the exact moment of damage occurrence. The increase in the decorrelation coefficient is more pronounced for #D and #E sensors, located behind the crack.

To better visualize the changes in DC over time of degradation, the moving reference trace function was used. Maps of $\mathbf{DC}^{mrt}$ vectors for beams #1–#3 and all sensors are shown in Fig. 7. The vectors are calculated for $k$ values at each time step and then compiled into the $\mathbf{DC}^{mrt,g}$ matrices. Calculations with the moving reference trace function made the moment of damage clearly visible on each map, regardless of the sensor selected.
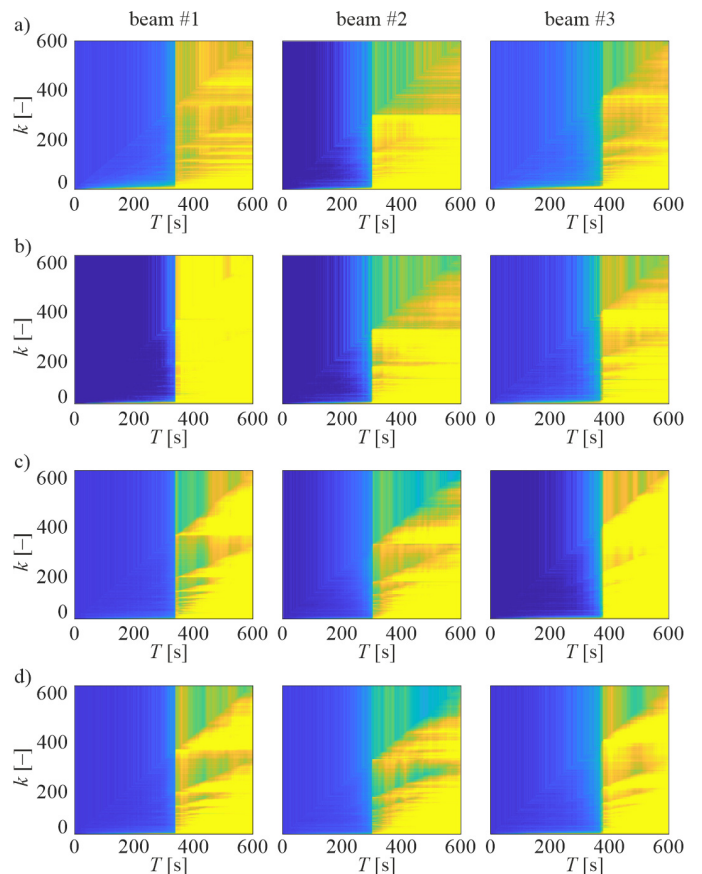


**Fig. 7.** Decorrelation maps of moving reference trace for beams #1–#3 and different sensors: a) sensor B, b) sensor C, c) sensor D, d) sensor E



**Fig. 6.** Decorrelation coefficient for beams #1–#3 and different sensors: a) sensor B, b) sensor C, c) sensor D, d) sensor E

Afterwards, the resulting matrices were averaged into single vectors. Figure 8 presents the values of $\mathbf{DC}^{mrt,g}$ matrices averaged over all steps $k$. First of all, the results for each beam
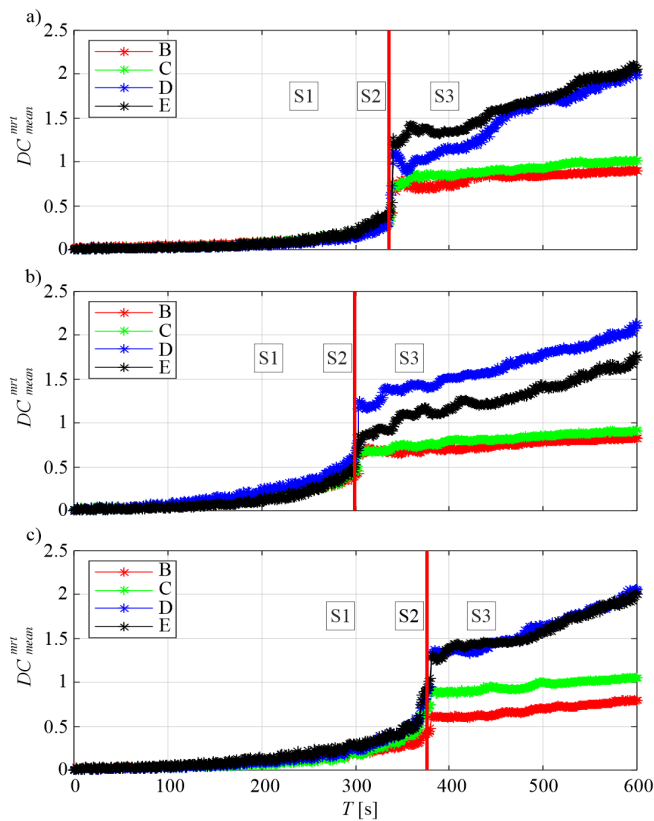
**Fig. 8.** Decorrelation diagrams of moving reference trace for mean values of $k = 1 : n$: a) beam #1, b) beam #2, c) beam #3

exhibit similar behavior. As in the results of the standard DC, for all sensors, three stages can be distinguished. Before reaching the destructive force, the decorrelation values for all sensors have small values. As the force increases, the average values increase, too. The sudden growth in the value of DC is noted at the moment of reaching the peak load value. After that, it is possible to distinguish between the sensors located in front of and behind the crack. After cracking, sensors B and C achieve stable decorrelation values. In contrast, sensors D and E are characterized by much higher and increasing values. There is a clear difference between the sensors in front of and behind the crack. In case the location of the damage is not known, this observation will help find the position of crack occurrence.

## 4. CONCLUSIONS

In this paper, monitoring of the fracture process of concrete beams was carried out by the application of integrated nondestructive methods. Optical and ultrasonic testing was used, enhanced by the processing of ultrasonic signals with the coda wave interferometry method.

First of all, similar mechanical behavior of all tested beams was observed. Digital image correlation allowed for successful visualization of the crack evolution. Moreover, the moment of formation of fracture process zones on the surfaces of samples was detected. Ultrasonic tests with coda wave interferometry provided information about the internal state of the samples.

This allowed for the detection of micro-cracks in beams before any symptoms appeared on the DIC maps. The moving reference trace approach allowed for better distinguishment of decorrelation coefficients calculated for signals from sensors in front of and behind a crack. This fact is promising for the further development of algorithms dedicated to crack localization.

In summary, the ultrasonic wave-based technique with coda wave interferometry processing appeared to prove itself as an effective technique for monitoring the fracture process and damage detection. Further works will extend the current study by using a greater number of sensors, which will allow for determining the position of the micro-crack zone based on the diffusive characteristics of collected signals.

## REFERENCES

[1] S. Zamen and E. Dehghan-Niri, "Fractal analysis of nonlinear ultrasonic waves in phase-space domain as a quantitative method for damage assessment of concrete structures," *NDT E Int.*, vol. 111, p. 102235, 2020, doi: 10.1016/j.ndteint.2020.102235.

[2] J. Chakraborty, A. Katunin, P. Klikowicz, and M. Salamak, "Early crack detection of reinforced concrete structure using embedded sensors," *Sensors*, vol. 19, no. 18, p. 3879, 2019, doi: 10.3390/s19183879.

[3] A. Deraemaeker and C. Dumoulin, "Embedding ultrasonic transducers in concrete: A lifelong monitoring technology," *Constr. Build. Mater.*, vol. 194, pp. 42–50, 2019, doi: 10.1016/j.conbuildmat.2018.11.013.

[4] M. Rucka, "Failure monitoring and condition assessment of steel-concrete adhesive connection using ultrasonic waves," *Appl. Sci.*, vol. 8, no. 3, p. 320, 2018, doi: 10.3390/app8030320.

[5] F. Moradi-Marani, P. Rivard, C.P. Lamarche, and S.A. Kodjo, "Evaluating the damage in reinforced concrete slabs under bending test with the energy of ultrasonic waves," *Constr. Build. Mater.*, vol. 73, pp. 663–673, 2014, doi: 10.1016/j.conbuildmat.2014.09.050.

[6] S. Lin, S. Shams, H. Choi, and H. Azari, "Ultrasonic imaging of multi-layer concrete structures," *NDT E Int.*, vol. 98, pp. 101–109, 2018, doi: 10.1016/j.ndteint.2018.04.012.

[7] Z.F. Tang, X.D. Sui, Y.F. Duan, P. Fei Zhang, and C.B. Yun, "Guided wave-based cable damage detection using wave energy transmission and reflection," *Struct. Control Heal. Monit.*, vol. 28, no. 5, p. e2688, 2021, doi: 10.1002/stc.2688.

[8] G. Vu, F. Diewald, J.J. Timothy, C. Gehlen, and G. Meschke, "Reduced order multiscale simulation of diffuse damage in concrete," *Materials*, vol. 14, no. 14, p. 3830, 2021, doi: 10.3390/ma14143830.

[9] G. Vu, J.J. Timothy, D.S. Singh, L.A. Saydak, E.H. Saenger, and G. Meschke, "Numerical simulation-based damage identification in concrete," *Modelling*, vol. 2, no. 3, pp. 355–369, 2021, doi: 10.3390/modelling2030019.

Coda wave interferometry in monitoring the fracture process of concrete beams under bending test

[10] C. Finger, L. Saydak, G. Vu, J.J. Timothy, G. Meschke, and E.H. Saenger, "Sensitivity of ultrasonic coda wave interferometry to material damage-observations from a virtual concrete lab," *Materials*, vol. 14, no. 14, p. 4033, 2021, doi: 10.3390/ma14144033.

[11] E. Ahn, M. Shin, J.S. Popovics, and R.L. Weaver, "Effectiveness of diffuse ultrasound for evaluation of micro-cracking damage in concrete," *Cem. Concr. Res.*, vol. 124, p. 105862, 2019, doi: 10.1016/j.cemconres.2019.105862.

[12] G. Sang, S. Liu, and D. Elsworth, "Quantifying fatigue-damage and failure-precursors using ultrasonic coda wave interferometry," *Int. J. Rock Mech. Min. Sci.*, vol. 131, p. 104366, 2020, doi: 10.1016/j.ijrmms.2020.104366.

[13] N. Smagin, A. Trifonov, O. Bou Matar, and V.V. Aleshin, "Local damage detection by nonlinear coda wave interferometry combined with time reversal," *Ultrasonics*, vol. 108, p. 106226, 2020, doi: 10.1016/j.ultras.2020.106226.

[14] E. Wojtczak, M. Rucka, and Ł. Skarżyński, "Monitoring the fracture process of concrete during splitting using integrated ultrasonic coda wave interferometry, digital image correlation and X-ray micro-computed tomography," *NDT E Int.*, vol. 126, p. 102591, 2022, doi: 10.1016/j.ndteint.2021.102591.

[15] H.J. Lim, H. Lee, T. Skinner, A. Chattopadhyay, and A. Hall, "Fatigue damage detection and growth monitoring for composite structure using coda wave interferometry," *Struct. Control Heal. Monit.*, vol. 28, no. 3, p. e2689, 2021, doi: 10.1002/stc.2689.

[16] M. Rucka, E. Wojtczak, M. Knak, and M. Kurpińska, "Characterization of fracture process in polyolefin fibre-reinforced concrete using ultrasonic waves and digital image correlation," *Constr. Build. Mater.*, vol. 280, p. 122522, 2021, doi: 10.1016/j.conbuildmat.2021.122522.

[17] J. Suchorzewski, M. Prieto, and U. Mueller, "An experimental study of self-sensing concrete enhanced with multi-wall carbon nanotubes in wedge splitting test and DIC," *Constr. Build. Mater.*, vol. 262, p. 120871, 2020, doi: 10.1016/j.conbuildmat.2020.120871.

[18] Ł. Skarżyński and J. Suchorzewski, "Mechanical and fracture properties of concrete reinforced with recycled and industrial steel fibers using Digital Image Correlation technique and X-ray micro computed tomography," *Constr. Build. Mater.*, vol. 183, pp. 283–299, 2018, doi: 10.1016/j.conbuildmat.2018.06.182.

[19] B. Gencturk, K. Hossain, A. Kapadia, E. Labib, and Y.L. Mo, "Use of digital image correlation technique in full-scale testing of prestressed concrete structures," *Meas. J. Int. Meas. Confed.*, vol. 47, no. 1, pp. 505–515, 2014, doi: 10.1016/j.measurement.2013.09.018.

[20] T.M. Fayyad and J.M. Lees, "Application of digital image correlation to reinforced concrete fracture," *Procedia Mater. Sci.*, vol. 3, pp. 1585–1590, 2014, doi: 10.1016/j.mspro.2014.06.256.

[21] D. Li *et al.*, "Experimental study on fracture and fatigue crack propagation processes in concrete based on DIC technology," *Eng. Fract. Mech.*, vol. 235, p. 107166, 2020, doi: 10.1016/j.engfracmech.2020.107166.

[22] G. Lacidogna, G. Piana, F. Accornero, and A. Carpinteri, "Multi-technique damage monitoring of concrete beams: Acoustic emission, digital image correlation, dynamic identification," *Constr. Build. Mater.*, vol. 242, p. 118114, 2020, doi: 10.1016/j.conbuildmat.2020.118114.

[23] Á.J. Molina-Viedma, L. Pieczonka, K. Mendrok, E. López-Alba, and F.A. Díaz, "Damage identification in frame structures using high-speed digital image correlation and local modal filtration," *Struct. Control Heal. Monit.*, vol. 27, no. 9, p. e2586, 2020, doi: 10.1002/stc.2586.

[24] X. Li, X. Chen, A. P. Jivkov, and J. Hu, "Investigation of tensile fracture of rubberized self-compacting concrete by acoustic emission and digital image correlation," *Struct. Control Heal. Monit.*, vol. 28, no. 8, p. e2744, 2021, doi: 10.1002/stc.2744.

[25] J. Singh and A. Curtis, "Estimating changes in velocity and source separation using coda wave interferometry: MATLAB code user guide," 2019.

*Bull. Pol. Acad. Sci. Tech. Sci.*, vol. 71, no. 3, p. e144118, 2023

7